Earth and Planetary Science Letters 577 (2022) 117242

Contents lists available at ScienceDirect

Earth and Planetary Science Letters

www.elsevier.com/locate/epsl

The role of preexisting upper plate strike-slip faults during long-lived (ca. 30 Myr) oblique flat slab subduction, southern Alaska

T.S. Waldien [a,e,*], R.O. Lease [b], S.M. Roeske [a], J.A. Benowitz [c], P.B. O'Sullivan [d]

[a] Department of Earth and Planetary Sciences, University of California, Davis, 1 Shields Ave., Davis, CA 95616, USA
[b] U.S. Geological Survey, Alaska Science Center, 4210 University Drive, Anchorage, AK 99508, USA
[c] Geophysical Institute, University of Alaska, Fairbanks, 900 Yukon Drive, Fairbanks, AK 99775, USA
[d] GeoSep Services, 1521 Pine Cone Road, Moscow, ID 83843, USA
[e] Department of Geology and Geological Engineering, South Dakota School of Mines and Technology, 501 E. St. Joseph St., Rapid City, SD 57701, USA

ARTICLE INFO

Article history:
Received 7 June 2021
Received in revised form 8 September 2021
Accepted 7 October 2021
Available online 27 October 2021
Editor: A. Webb

Keywords:
oblique
subduction
transpression
thermochronology
detrital
Yakutat

ABSTRACT

Upper plates of subduction zones commonly respond to flat slab subduction by structural reactivation, magmatic arc disruption, and foreland basin inversion. However, the role of active strike-slip faults in focusing convergent deformation and magmatism in response to oblique flat slab subduction remains less clear. Here, we present new detrital apatite fission-track (dAFT) ages from 12 modern catchments in the eastern Alaska Range, Alaska, USA, to reveal how the dextral Denali fault system has facilitated bedrock exhumation and topographic growth during ca. 30 Ma-to-present oblique flat slab subduction of the Yakutat oceanic plateau. Additionally, a 940 ka ($^{40}Ar/^{39}Ar$ whole rock) basalt flow is spatially associated with Cenozoic structures, locally reset AFT ages and provides the first evidence for Quaternary volcanism along the southern flank of the eastern Alaska Range. We integrate our new data with other thermochronologic, geochronologic, and regional geologic datasets to show that (1) most high topography regions in southern Alaska have undergone rapid bedrock cooling and exhumation since ca. 30 Ma; (2) elevated terrain and young cooling are spatially associated with long-lived active strike-slip fault systems; (3) topographic growth associated with strike-slip fault deformation led to local inversion of basin systems and drainage reorganization; (4) the onset of oblique oceanic plateau subduction is coeval with a southward shift in arc magmatism from one region of active strike-slip faulting to another above the northeastern edge of the flat slab; and (5) Quaternary volcanism marks the revival of magmatism in the eastern Alaska Range above the geophysically imaged northeastern edge of the flat slab. Our analysis of the post-30 Ma geologic evolution of southern Alaska demonstrates that strike-slip fault systems that were active at the time of slab flattening evolved into transpression zones that focused bedrock cooling, rock exhumation, and topographic growth.

1. Introduction

Active deformation at plate boundaries involving continental lithosphere commonly deviates from plate-like behavior (e.g., Freymueller, 2010). Spatially distributed deformation is clearly evident in flat slab subduction environments where increased upper plate convergence associated with slab flattening can drive widespread upper plate deformation hundreds of kilometers inboard of the trench (e.g., Axen et al., 2018). Distributed fault reactivation, basin inversion, and migration of the magmatic arc are considered hallmarks of upper plate tectonic evolution in both modern flat slab regions of South America (Ramos et al., 2002) and inferred ancient flat slab regions of North America (Saleeby, 2003). The down-dip extent of increased plate boundary coupling (Espurt et al., 2008), end loading (Axen et al., 2018), and locations of inherited major crustal structures (Marshak et al., 2000) are thought to primarily control the degree to which upper plate shortening is localized or distributed. Minor strike-slip structures have been shown to form perpendicular to the plate boundary as part of the upper plate shortening regime in response to the subduction of buoyant crust (e.g., Gardner et al., 2013). However, the role of pervasive, large-magnitude strike-slip faulting in oblique flat slab environments has received relatively little attention to date. Here, we investigate how preexisting active continental strike-slip fault systems influence the distribution of upper plate deformation and magmatism in the long-lived oblique flat slab subduction setting of southern Alaska.

* Corresponding author at: Department of Geology and Geological Engineering, South Dakota School of Mines and Technology, 501 E. St. Joseph St., Rapid City, SD 57701, USA.
E-mail address: trevor.waldien@sdsmt.edu (T.S. Waldien).

https://doi.org/10.1016/j.epsl.2021.117242

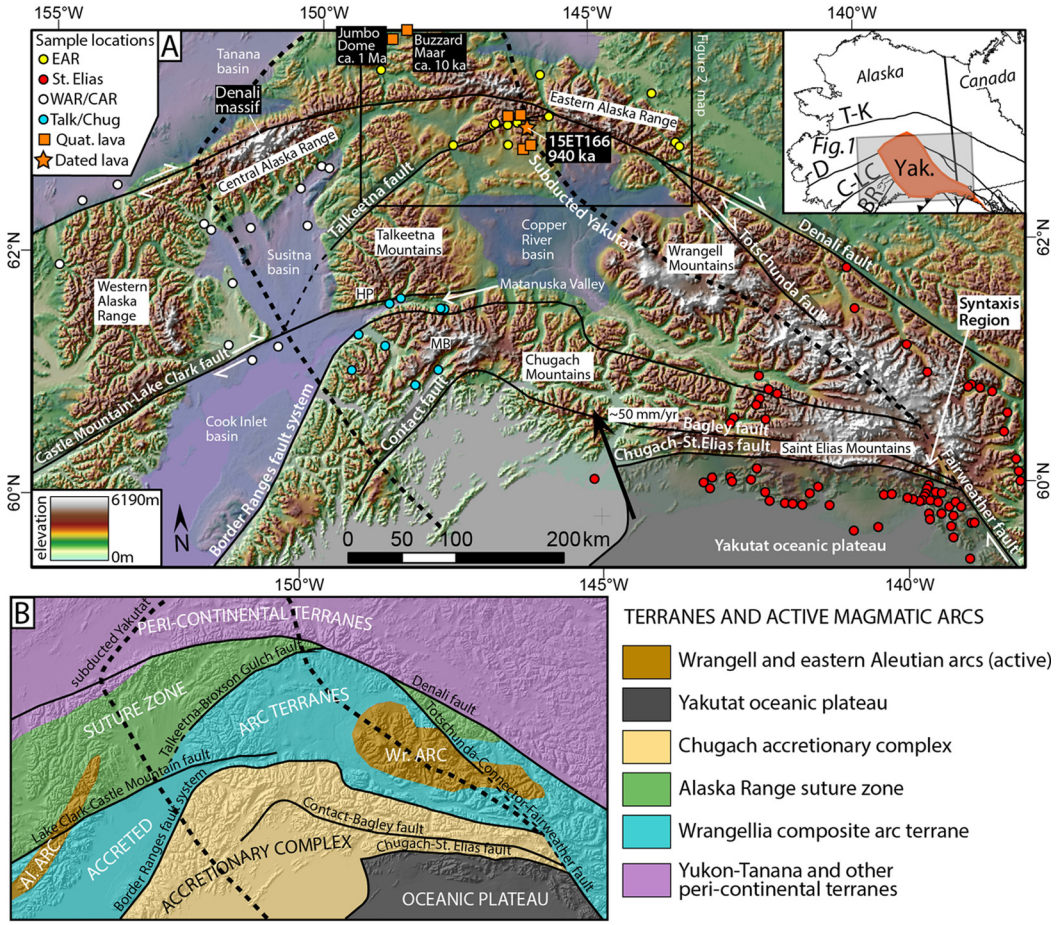

Fig. 1. A) Shaded relief map of southern Alaska showing new and compiled modern river detrital fission-track sample locations (colored circles) and locations of Alaska Range Quaternary (Quat.) volcanic fields (orange squares and star) relative to major structures (black lines) and basins (blue shaded regions). The exposed Yakutat oceanic plateau (transparent-black shaded region) and flat-slab subducted extent (broken bold black line from Pavlis et al., 2019) is inferred to drive upper plate deformation in southern Alaska. Relative motion between the Yakutat block and southern Alaska is represented by the bold black arrow. HP–Hatcher Pass; MB–Mount Marcus Baker; WAR–Western Alaska Range; CAR–Central Alaska Range; EAR–Eastern Alaska Range; Chug–Chugach Mountains; Talk–Talkeetna Mountains. Faults in inset: T-K–Tintina-Kaltag; D–Denali; C-LC–Castle Mountain-Lake Clark; BR–Border Ranges; Yak-subducted extent of Yakutat oceanic plateau (orange). **B)** Hillshade map of the same extent as Fig. 1A overlain by terrane geology (see section 2 for details). Colored domains are labeled generically on the map and represent generalized southern Alaska terranes in the legend. (For interpretation of the colors in the figure(s), the reader is referred to the web version of this article.)

Subduction of the Yakutat oceanic plateau (Christeson et al., 2010) beneath southern Alaska is a prolonged, and still active, example of a flat slab environment wherein the upper plate is dissected by numerous inherited strike-slip faults (Finzel et al., 2011a; Allam et al., 2017). Flat slab subduction is inferred to have begun by ca. 30 Ma based on modification of the upper plate thermal structure, migration of arc magmatism, and topographic growth at that time (Enkelmann et al., 2015 and references therein; Brueseke et al., 2019; Trop et al., 2019). Long-lived (ca. 30 Myr) and still active upper plate dextral strike-slip faults in southern Alaska include the Denali, Castle Mountain-Lake Clark, eastern Contact-Bagley, Totschunda, and Fairweather fault systems (Fig. 1).

Geophysical models of southern Alaska deformation yield variable importance of strike-slip fault systems in regional deformation above the flat slab. Despite generally sparse coverage of GPS stations in southern Alaska (e.g., Freymueller et al., 2008; Elliott and Freymueller, 2020), the geodetic velocity field and distribution of crustal seismicity together highlight the strike-slip fault systems as zones of focused deformation (Ruppert et al., 2008). Inverse numerical simulations of the geodetic velocity field suggest a somewhat different view wherein the strike-slip fault systems occupy zones of elevated strain rate embedded into regionally diffuse deformation above the flat slab (Finzel et al., 2011b). Alternatively, finite element forward geodynamic modeling favors high coupling between the subducted flat slab and base of the upper plate, which would act to increase the strength of the upper plate by refrigeration and mechanical thickening (Koons et al., 2010; Jadamec et al., 2013). In the forward simulations, lateral rheological contrasts in the upper plate (e.g., lithospheric scale strike-slip faults) are crucial for focusing upper plate deformation. More recent block-modeling of geodetic data suggests an intermediate scenario wherein the size of the blocks, and thus the potential for deformation localization, increases with distance from the plate boundary (Elliott and Freymueller, 2020). A potential implication of the block modeling is that the role of preexisting strike-slip fault systems in focusing upper plate deformation increases with distance from the plate boundary fault system.

In this contribution, we assess the role of preexisting upper plate strike-slip faults in the oblique flat slab environment of southern Alaska by evaluating regional exhumation patterns through the lens of detrital thermochronology. Studies using detrital mineral chronometers from modern sediment and Neogene-Quaternary stratigraphic sections have proven foundational for understanding long-term patterns of bedrock cooling, erosion, and magmatism in largely inaccessible regions of southern Alaska (e.g., Enkelmann et al., 2019). Detrital thermochronology data are par-

ticularly well suited to capture regional exhumational responses to changes in plate boundary forcing due to the spatial-temporal sensitivity of the technique to tectonic events affecting broad regions. Here, we present modern river detrital apatite fission-track (dAFT) data from 12 catchments in the eastern Alaska Range (yellow circles in Fig. 1). We compare the new dAFT data to published dAFT and detrital zircon fission-track (dZFT) datasets sampled from modern catchments in other regions across southern Alaska (red, blue, and white circles in Fig. 1) to evaluate whether deformation is diffuse across the upper plate of the flat slab region, or primarily focused along preexisting strike-slip fault systems. Additionally, we present the first field observations and an $^{40}Ar/^{39}Ar$ date documenting a newly recognized Quaternary volcanic field in the eastern Alaska Range, which has perturbed bedrock cooling in the region. Our integration of new and published data reveals loci of Oligocene-to-Neogene upper plate deformation and topographic growth, which inform a comprehensive model describing the tectono-magmatic response to oblique flat slab subduction of the Yakutat oceanic plateau beneath southern Alaska.

2. Regional geology and cooling patterns in southern Alaska

Much of the geology of the northern North American Cordillera formed by accretion of tectonostratigraphic terranes during the Mesozoic. From north to south, important terranes in southern Alaska include peri-continental Laurentian metamorphic rocks north of the Denali fault, the Wrangellia composite island arc terrane south of the Denali fault, and the Chugach accretionary complex south of the Border Ranges fault system (Fig. 1B). The boundaries between these terranes are in most places occupied by dextral strike-slip faults that are interpreted to penetrate the lithosphere based on receiver function seismology (e.g., Miller et al., 2018) and seismic anisotropy studies (e.g., Estéve et al., 2020). The Denali fault system juxtaposes the accreted Wrangellia arc terrane in the south against continental North American-affinity terranes to the north. A region underlain by imbricated Mesozoic marginal marine basin strata, plutonic rocks, oceanic fragments, and disparate continental terranes known as the Alaska Range suture zone is intersected by the Denali fault and appears to focus post-suturing deformation (Fitzgerald et al., 2014), which facilitated rapid Neogene exhumation of the Alaska Range (Haeussler et al., 2008; Benowitz et al., 2014; Lease et al., 2016). South of the Wrangellia terrane, the Chugach accretionary complex represents the forearc to Mesozoic arcs that were built upon the Wrangellia composite terrane, although the accretionary complex has been translated hundreds of kilometers from the associated arc rocks by Late Cretaceous-Paleogene dextral slip along the Border Ranges fault system (e.g., Roeske et al., 2003). Oligocene to present exhumation of the accretionary complex is largely associated with underplating of the Yakutat slab along with its cover strata and is mainly facilitated by transpression along the Contact fault system in the western Chugach Range and the Bagley fault in the eastern Chugach Range (Bruhn et al., 2012; Arkle et al., 2013).

Low-temperature cooling patterns across southern Alaska suggest that bedrock cooling has taken place in response to regional magmatic, tectonic, and climatic forcing. Late Cretaceous cooling can be attributed to exhumation and/or thermal relaxation following accretion of the Wrangellia composite terrane to western North America (Falkowski and Enkelmann, 2016; McDermott et al., 2019). Early Cenozoic cooling is widespread throughout southern Alaska and adjacent Yukon and likely records extension (e.g., O'Sullivan and Currie, 1996), post-magmatic cooling of batholithic rocks (Lease et al., 2016; Enkelmann et al., 2019), and/or a possible slab window event (Terhune et al., 2019). Cooling age data from high elevation regions commonly show an increase in cooling rate at ca. 25-30 Ma, which is generally considered to record flattening of the Yakutat slab (Finzel et al., 2011a; Enkelmann et al., 2015; Lease et al., 2016). The onset of alpine glaciation in Alaska at ca. 4 Ma (Gulick et al., 2015; Horikawa et al., 2015) enhanced bedrock erosion in high elevation regions and is recorded in low-temperature cooling age data regionally (e.g., Berger et al., 2008; Lease, 2018).

3. Methods

3.1. Apatite fission-track thermochronology

New dAFT data reveal the $\leq$110 °C cooling history of 12 catchments spanning 330 km of the eastern Alaska Range (Fig. 2). Samples comprise several subsamples of medium-coarse sand collected from gravel bars along a 10-100 m river length to ensure a representative, well-mixed sample. In 2019, sample collection involved heavy mineral concentration in the field using a miner's gold pan and further concentration at UC Davis using standard magnetic and density techniques. Apatite concentration from samples collected prior to 2019 took place at GeoSep Services using standard magnetic and density separation techniques. Fission-track dating at GeoSep Services involved counting spontaneous fission tracks on 70-110 grains per sample and parent isotope ratio measurement using the laser ablation inductively coupled plasma mass spectrometer (LA-ICP-MS) method (Donelick et al., 2005) at Washington State University (detailed methods in Appendix A and data in Appendix B). We filtered the dAFT data and rejected analyzed grains if they exhibited a uranium concentration less than 0.5 ppm and an AFT age that is not within uncertainty of the oldest known bedrock crystallization age in the catchment (<2% of the total dataset). We deconvolved the dAFT datasets into constituent age populations for each catchment (Fig. 2; Table 1) using the mixture modeling methods available in DensityPlotter v. 8.4 (Vermeesch, 2012).

We compared the new and existing modern river dAFT and dZFT datasets cross southern Alaska based on the abundance and proportions of constituent age populations in different regions (Fig. 3). We compiled the resolved age components for each detrital fission-track sample analyzed within a region and generated probability density plots of the age population data for each region. Because the age population plots do not account for the proportion of dated grains that constitute each age population, we augment the probability density plots with pie charts that show the data binned into regionally important time intervals (<4, 4-30, and >30 Ma) and weighted by the proportion of dated grains in those time bins.

3.2. $^{40}Ar/^{39}Ar$ geochronology

$^{40}Ar/^{39}Ar$ analysis performed on one basalt sample at the Geochronology laboratory at the University of Alaska, Fairbanks, involved crushing the sample, sieving for the 500-1000 μm fraction, washing dust from the fraction, and handpicking for a pure phase of phenocryst-free groundmass. Monitoring of the neutron flux and calculation of the irradiation parameter (J) were based on the monitor mineral TCR-2 with an age of 28.619 Ma (Renne et al., 2010). See Appendix C for detailed $^{40}Ar/^{39}Ar$ methods and data.

4. Results: new and compiled data

4.1. New detrital fission-track data

Individual catchments in the eastern Alaska Range predominantly yield AFT age populations at ca. 8-15 Ma, 20-30 Ma, and 50-65 Ma (Fig. 2; Table 1). The middle and west forks of the Maclaren River contain small (~5% abundance) populations centered

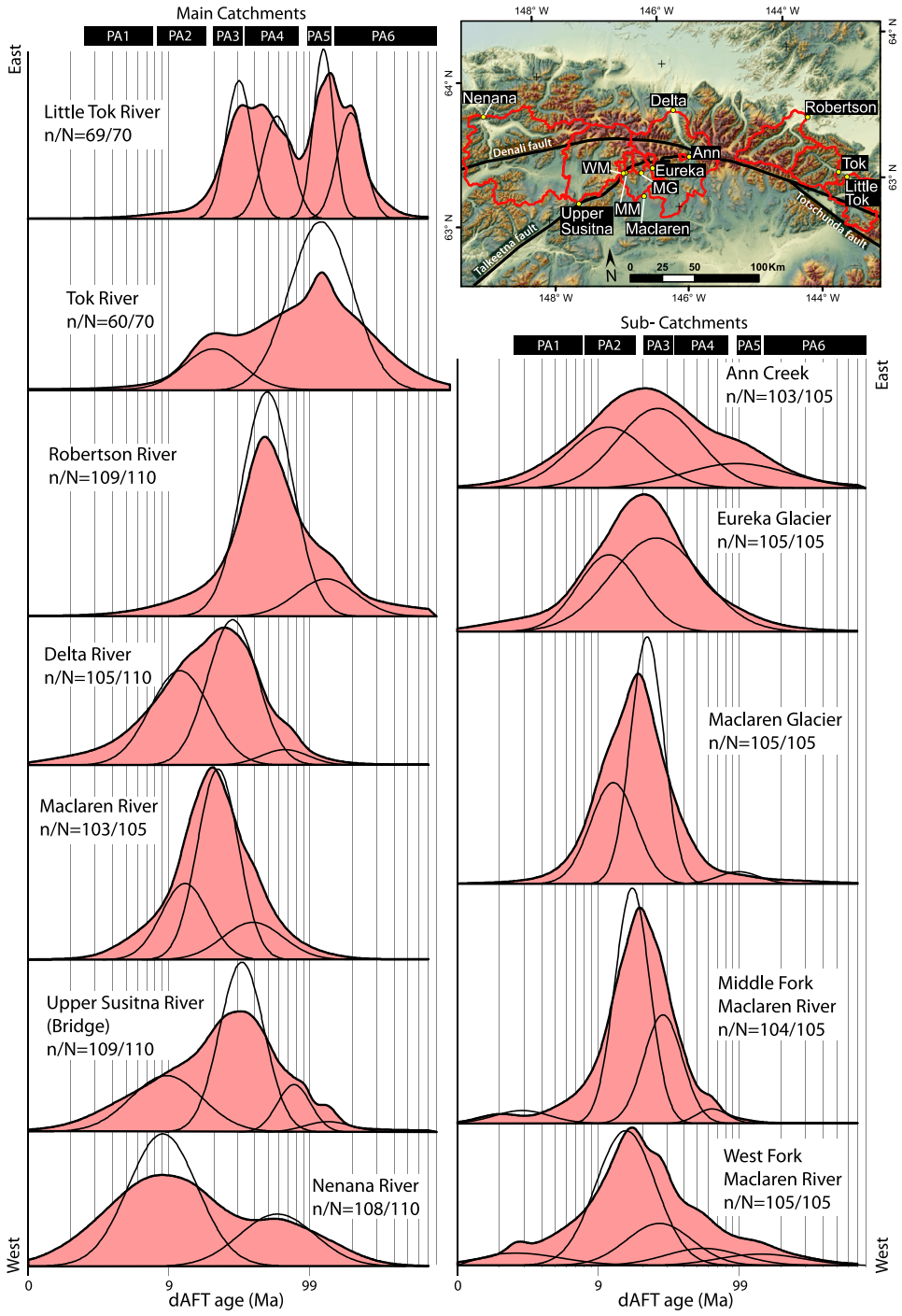

Fig. 2. Equal-area probability density plots (PDPs) of detrital apatite fission-track data from individual catchments in the eastern Alaska Range. Filled PDPs represent the entire mixed dataset, whereas unfilled black PDPs represent unmixed age populations. A logarithmic scale is used for single-grain age distributions because of Poisson counting statistics and large, variable, and asymmetric uncertainties (Galbraith, 2005). The inset map in the upper right shows the locations of the catchments. *N*–total number of analyzed grains; *n*–number of grains used in the unmixing analysis; PA1-6–Apatite fission track age populations defined in Table 1. Abbreviated catchment names: WM–West Fork Maclaren River; MM–Middle Fork Maclaren River; MG–Maclaren Glacier.

at ca. 1.6-1.9 Ma, and several catchments also yield older (>90 Ma) age populations.

The combined dAFT dataset ($n = 1210$ single-grain dates) for catchments in the eastern Alaska Range presented herein records widespread Cenozoic cooling (Fig. 3A). Of the dated grains, ~69% document cooling between 4-30 Ma, and resolved age populations are present at ca. 8-12 Ma and 22-28 Ma. Approximately 30% of the grains record cooling between 30-197 Ma, and the remaining ~1% record cooling since 4 Ma.

4.2. Compiled detrital fission-track data

Modern river detrital fission-track data from the western/central Alaska Range compiled here from Lease et al. (2016), Finzel et al. (2016), and Enkelmann et al. (2019) display multiple phases of Cenozoic cooling (Fig. 3B). The combined dAFT dataset predominantly records cooling from 30-4 Ma, wherein ~46% of the dated grains fall into age populations at ca. 20-25 Ma and 6-10 Ma. Approximately 17% of the dated apatite grains record cooling younger

Table 1
Eastern Alaska Range detrital apatite fission-track age populations.

Sample	Sample collection (year)	PA1 (1.6-7 Ma)	PA2 (7-17 Ma)	PA3 (20-33 Ma)	PA4 (38-77 Ma)	PA5 (96-134 Ma)	PA6 (≥145 Ma)	$n^a(N)^b$
Ann Creek	2019		10.9 ± 2.7 (35%)	25.7 ± 4.8 (47%)		96 ± 19 (18%)		103(105)
Eureka Glacier	2019		11.1 ± 1.7 (36%)	25.2 ± 2.5 (64%)				105(105)
Maclaren Glacier	2019		11.9 ± 1 (35%)	21.4 ± 1.1 (62%)		99 ± 31 (3%)		105(105)
M. Fork Maclaren R.	2019	1.9 ± 0.6 (5%)	16.6 ± 0.8 (61%)	28.1 ± 1.6 (31%)	63.9 ± 7.7 (3%)			104(105)
W. Fork Maclaren R.	2019	1.6 ± 0.4 (4%)	14.9 ± 0.9 (60%)	26.6 ± 2.6 (21%)	55.9 ± 8.5 (9%)		145 ± 28 (6%)	105(105)
Maclaren River	2019		12 ± 1.2 (26%)	21.3 ± 1.4 (57)	38.5 ± 4.8 (17%)			103(105)
Little Tok River	2016			30.6 ± 2.1 (29%)	57.9 ± 3.4 (23%)	125.3 ± 5.2 (26%)	197 ± 12 (21%)	69(70)
Robertson River	2012				49.8 ± 2.3 (84%)	133 ± 14 (16%)		109(110)
Delta River	2014		11.1 ± 1.3 (41%)	27.6 ± 1.9 (54%)	66.1 ± 7.7 (5%)			105(110)
Upper Susitna River	2014		8.6 ± 1.3 (30%)	32 ± 2 (56%)	76.3 ± 7.5 (11%)	134 ± 15 (3%)		109(110)
Tok River	2016			20 ± 4.5 (18%)		119 ± 14 (82%)		60(70)
Nenana River	2014		7.8 ± 0.6 (73%)		65.5 ± 6.9 (27%)			108(110)

[a] *n*–number of analyzed grains used in unmixing.
[b] *N*–total number of analyzed grains. Uncertainties on population ages are 1 s. Percentages are proportions of each component age population as part of the entire dataset.

than 4 Ma, which is linked to enhanced glacial erosion in the high relief region during the middle to late Pliocene (Lease, 2018). Detrital zircon fission-track data from the same catchments do not contain age populations younger than 4 Ma, yet ~37% of the dZFT cooling ages form an age population at ca. 15-30 Ma. Both the combined dAFT and dZFT datasets record significant (dAFT~37% and dZFT~63%) bedrock cooling older than 30 Ma, which can be correlated with regional magmatic/thermal events (Lease et al., 2016; Terhune et al., 2019; Regan et al., 2020).

Modern river and proglacial dZFT data from the northern Chugach Mountains (Arkle et al., 2013) and southern Talkeetna Mountains (Enkelmann et al., 2019) display a spectrum of Cenozoic cooling ages (Fig. 3C). The majority (~82%) of the dated grains record cooling at ca. 45 and 65 Ma, which can be correlated to magmatic/thermal events at those times (Terhune et al., 2019), and/or unroofing in nearby portions of the ranges (Little and Naeser, 1989; Trop and Ridgway, 2007). Post-30 Ma cooling is recorded in the remaining ~37% of the dated grains, which primarily compose a ca. 22-29 Ma age population.

Modern river detrital fission-track data from catchments draining the northern flank of the St. Elias Mountains published by Enkelmann et al. (2015 and references therein) and Falkowski and Enkelmann (2016) record cooling that spans the Cretaceous and Cenozoic (Fig. 3D). The majority (~53% dAFT and ~80% dZFT) of the dated grains record bedrock cooling older than 30 Ma, which is interpreted to reflect cooling during terrane accretion and multiple pulses of regional magmatism (Falkowski and Enkelmann, 2016). Cooling from 30-4 Ma is recorded by ~39% of the compiled dAFT data and ~20% of the dZFT data. The 30-4 Ma cooling ages are present in the catchments that intersect the high peak region of the St. Elias Mountains and thus may record focused cooling within the retrowedge of the orogen (e.g., Falkowski et al., 2014). Cooling younger than 4 Ma is mainly recorded in the dAFT data (8% of the dated grains) and likely records enhanced glacial erosion in the region of Mt. Logan (Enkelmann et al., 2015 and references therein).

Modern river and proglacial detrital fission-track data from catchments draining the southern flank of the St. Elias Mountains compiled by Enkelmann et al. (2015) record widespread late Cenozoic cooling in the upper plate proximal to the Yakutat collision zone (Fig. 3E). The comparable proportions of <4 Ma (46%) and 4-30 Ma (45%) grains in the compiled dAFT data indicate that enhanced glacial erosion and tectonically driven exhumation work in tandem to generate the high relief of the St. Elias Mountains (e.g., Berger et al., 2008). The remaining ~9% of dAFT grains fall into a distributed age range as old as ca. 128 Ma. Detrital ZFT data from the same catchments predominantly record cooling older than 30 Ma (65% of the dated grains), yet those grains do not cluster into discrete age populations. Younger, discrete dZFT age populations are present at ca. 25 Ma, 18 Ma, and younger than 10 Ma, which together compose ~23% of the analyzed grains. Cooling younger than 4 Ma is recorded by ~12% of the dated zircon grains, which suggests that the combined tectonic forcing and glacial erosion was locally significant enough to exhume rocks from below the ZFT closure temperature (~240 °C) since 4 Ma.

Table 2
Locations of young volcanic features south of the Eastern Alaska Range.

Feature	LAT (°N)	LONG (°W)
Scoria	63.1358	146.3252
Blocky lava flow	63.1371	146.3217
Possible tuff interbedded with lava	63.0553	146.3132
Platey lava	63.0547	146.3110
Oxidized lavas- possible vent	63.0569	146.3125
15ET166- Platey lava	63.2357	146.1944
Cinder	63.1364	146.3199

4.3. Quaternary volcanism in the eastern Alaska Range

We present the first description of Quaternary volcanic rocks along the southern flank of the eastern Alaska Range. Stout (1976) mapped isolated exposures of "Tertiary basalt flows" that unconformably overlie older structures in the area. Based on the recent recognition that many of the structures beneath the basalt flows have post-Oligocene slip (Twelker et al., 2020; Waldien et al., 2021a), the field relationships alone suggest that the basalt flows are Neogene or younger. We dated one outcrop of olivine basalt near the southern flank of the eastern Alaska Range (orange star on Fig. 1), which yielded an $^{40}Ar/^{39}Ar$ whole rock plateau age of 940.4 ± 27.1 ka (Fig. 4A). In addition to the dated locale, our reconnaissance fieldwork has revealed additional outcrops of similar, potentially younger lavas where delicate flow features and rock types including brecciated flow tops and scoria are locally preserved. Owing to their low preservation potential, the presence of scoria, cinder, and volcanic landforms implies that portions of the Quaternary volcanic field along the southern flank of the Alaska Range may be younger than the regional Pleistocene glaciations. Table 2 and Fig. 4 contain locations and photos of features in the Quaternary volcanic field.

5. Discussion

5.1. Regional integration of thermochronology datasets

The new dAFT data from the eastern Alaska Range augment existing bedrock and detrital thermochronology datasets from southern Alaska indicating a major shift in the regional tectonic frame-

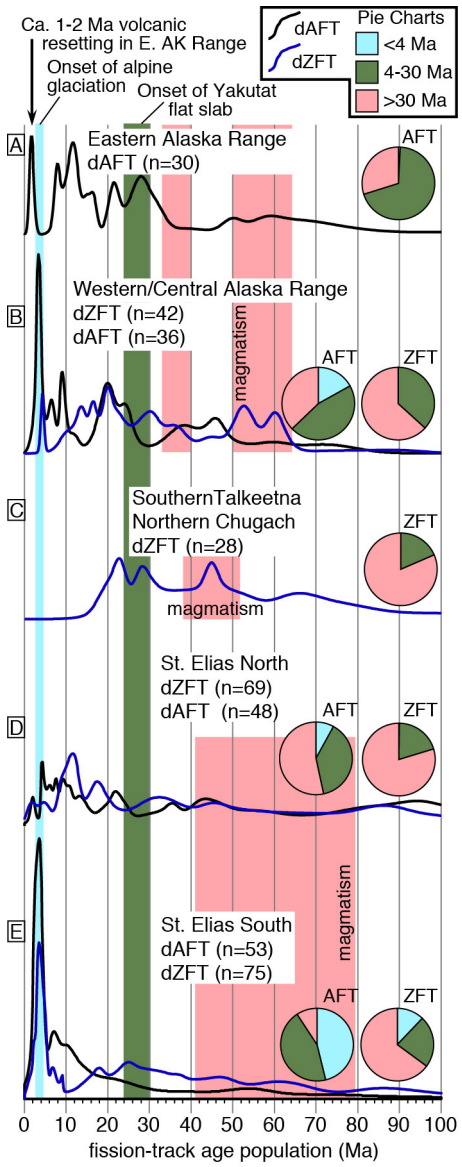

Fig. 3. Equal-area probability density plots of compiled modern river detrital apatite and zircon fission-track age populations from (A) the eastern Alaska Range (this study), (B) western/central Alaska Range, (C) southern Talkeetna and northern Chugach Mountains, and (D and E) St. Elias Mountains (see Section 4.2 for references). Pie charts summarize the age populations normalized by their proportions of the entire single grain dataset and binned into <4 Ma, 4-30 Ma, and >30 Ma time intervals. Red shaded time intervals represent times of known magmatism in each region and green/blue shaded time intervals represent known times of regional cooling events. dAFT–detrital apatite fission-track; dZFT-detrital zircon fission track; *n*–number of age populations used in the plots.

work at ca. 30 Ma (Benowitz et al., 2014; Riccio et al., 2014; Lease et al., 2016; Waldien et al., 2021a). Assessing the dAFT data from the entire Alaska Range reveals that ~50% of detrital apatite grains record cooling since 30 Ma and that tectonic-related cooling in that time frame may be further split into populations at ca. 28, 20-22, and 8-12 Ma (Fig. 3A-B). Quaternary cooling ages in the eastern Alaska Range dataset are ca. 1.5 Myr younger than cooling attributed to enhanced glacial erosion in the central/western Alaska Range (Figs. 2 and 3A-B) and are limited to two catchments that contain relatively unweathered basalt clasts near the newly identified Quaternary volcanic field (Figs. 1, 4F). On the basis of the above observations, we attribute the Quaternary AFT dates in the eastern Alaska Range to reflect volcanic provenance, annealing of apatite fission tracks from interaction with volcanic fluids, and/or the thermal effects associated with the newly identified Quaternary volcanism in the region.

In the western and central Alaska Range, both the dAFT and dZFT datasets record Oligocene-Neogene cooling (Fig. 3B). Post-30 Ma events in the Alaska Range that may have facilitated cooling include exhumation related to thrust reactivation of terrane accretionary structures (Waldien et al., 2021a), waning magmatism along the Denali fault (Trop et al., 2019; Regan et al., 2021), and rock uplift associated with restraining bends along the Denali fault (Fitzgerald et al., 2014). Heterogeneity in the major cooling age populations among catchments (Figs. 2 and 3; Table 1) suggests that cooling, exhumation, and related topographic growth in the Alaska Range were not uniform across the entire range. Instead, variation in the location, rate, and episodicity of rock uplift/exhumation are more probable (e.g., Bill et al., 2018) and may be related to a spatially variable structural and kinematic evolution of the Denali fault system (e.g., Waldien et al., 2018).

Both bedrock and detrital thermochronology datasets display abundant post-30 Ma cooling and exhumation in mountainous regions across southern Alaska (Figs. 3 and 5). Bedrock cooling ages suggest Oligocene-to-present exhumation depths of ≥14 km north of the Denali fault in the eastern Alaska Range (Benowitz et al., 2014), ≤10 km south of the Denali fault in the eastern Alaska Range (Waldien et al., 2018, 2021a), <6 km south of the Denali fault in the Kluane Ranges (McDermott et al., 2019), >8.5 km in the Denali massif (Fitzgerald et al., 1995), >6 km in the western Alaska Range south of the Denali fault (Lease, 2018), 5-11 km in the central Chugach Mountains (Arkle et al., 2013), ≤4 km in the Talkeetna Mountains (Terhune et al., 2019), and ≤10 km depth in the St. Elias Mountains (Enkelmann et al., 2015 and references therein). Assuming a paleo-geothermal gradient of ~30 °C/km, a ZFT closure temperature of 240 °C, and that clustering of single-grain dZFT dates records cooling from below the ZFT partial retention zone, the dZFT data compiled herein suggest that most high-elevation regions of southern Alaska have, at least locally, experienced bedrock exhumation from depths of ≥8 km. The bedrock and detrital cooling age data together suggest, aside from elements of paleo-topography in the Talkeetna Mountains (Terhune et al., 2019; Fig. 5), the western Alaska Range (Benowitz et al., 2012), and portions of the northern St. Elias Mountains (Falkowski and Enkelmann, 2016), that the topographic signature of southern Alaska has largely taken form since ca. 30 Ma.

5.2. Oligocene-to-present arc magmatism in southern Alaska

The Oligocene marks a fundamental shift in the loci of arc magmatism in southern Alaska. U-Pb zircon dating from exhumed batholithic rocks and modern river sands indicates that prior to ca. 32 Ma, the Alaska Range was the locus of Cenozoic subduction-related magmatism (Lease et al., 2016; Regan et al., 2020, 2021; Jones et al., 2021). From ca. 32-25 Ma, arc magmatism waned in the Alaska Range (Trop et al., 2019) and refocused in the region of the present-day Wrangell Mountains, which contain calc-alkaline igneous rocks as old as ca. 30 Ma (Brueseke et al., 2019). The migration of arc magmatism led to a magmatic gap throughout the eastern and central Alaska Range between the eastern Aleutian and Wrangell Mountains arcs, which broadly aligns with the present-day subducted extent of the Yakutat slab (Jones et al., 2021; Fig. 1).

Although ca. 2-25 Ma igneous rocks are absent from the eastern and central Alaska Range, the presence of Quaternary volcanic fields along the southern (940.4 ± 27.1 ka lava flow; Fig. 4) and northern (Jumbo Dome–1.026 ± 0.057 Ma [$^{40}Ar/^{39}Ar$ hornblende]; Cameron et al., 2015, and Buzzard Maar–ca. 10 ka [$^{40}Ar/^{39}Ar$ groundmass]; Andronikov and Mukasa, 2010) flanks of the Alaska

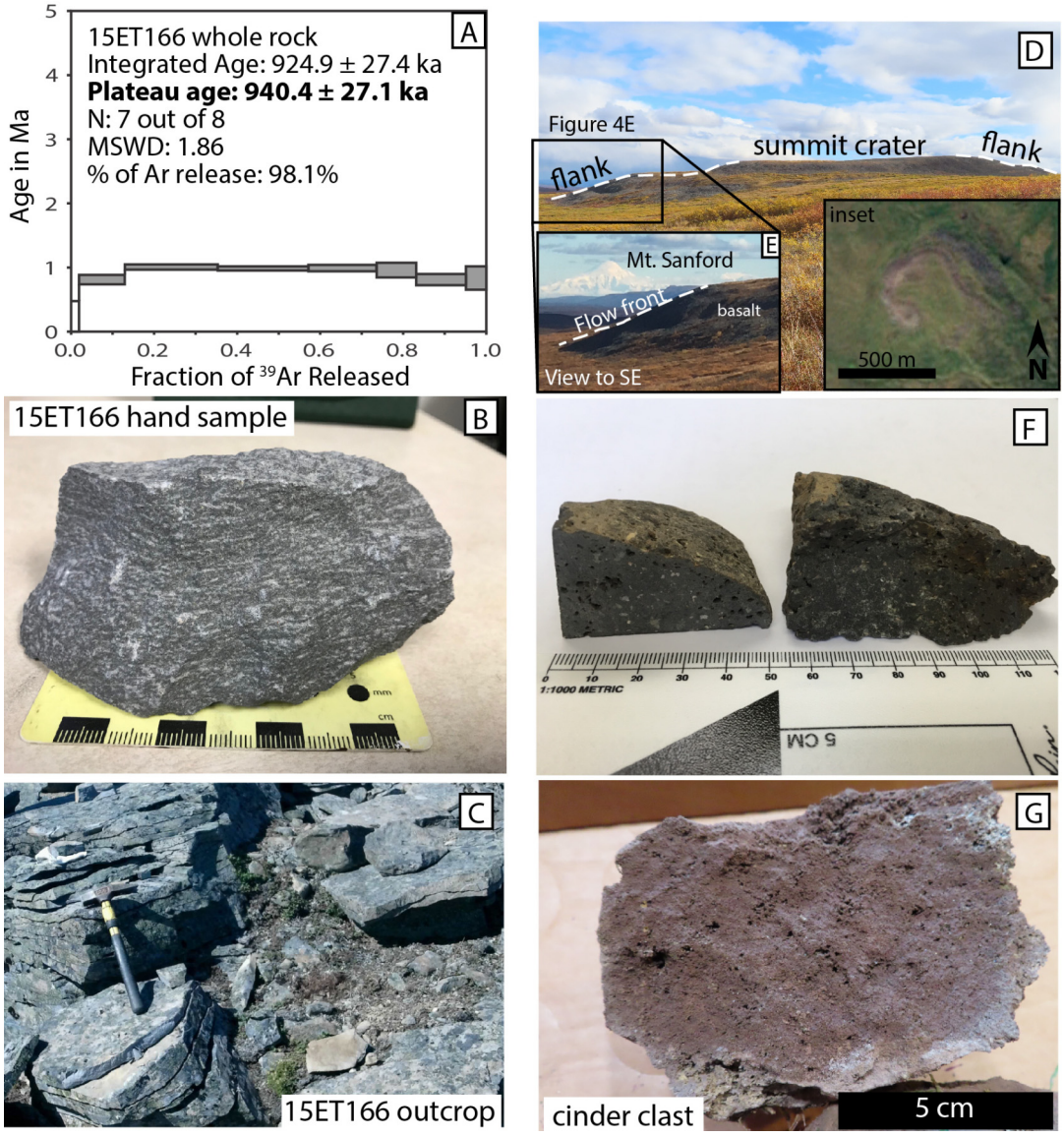

Fig. 4. Features of Quaternary volcanic rocks in the eastern Alaska Range. **A)** $^{40}Ar/^{39}Ar$ age spectrum for sample 15ET166. Gray-filled gas release steps are used to calculate the age of the sample. *N*–number of gas release steps used to calculate the age; MSWD–mean square weighted deviation. **B)** 15ET166 hand sample. Photo by Evan Twelker (Alaska Division of Geology and Geological Surveys). **C)** Outcrop photo of 15ET166 (orange star on Fig. 1). The platy outcrop pattern pictured here is common among outcrops of young volcanic rocks in the eastern Alaska Range. The hammer for scale is ~40 cm long. Photo by Evan Twelker (Alaska Division of Geology and Geological Surveys). **D)** Geomorphic features indicative of young volcanism are preserved in the landscape. Here, a semi-conic feature composed of oxidized basalt is preserved. ***Inset***: Google Earth image showing that the cone appears to have breached out of the southeast flank ("cinder cone" in Table 2). **E)** Zoomed-in image of the cone flank illustrating the along-strike relationship with the Wrangell arc (Mt. Sanford). **F)** Vesicular basalt clasts are locally present in glacial outwash. This sample was collected from a moraine adjacent to the Eureka Glacier. **G)** A late Pleistocene, or potentially post-glacial Holocene, age for some volcanic features is suggested by the presence of unaltered cinder ejecta (pictured here from "cinder cone" coordinate in Table 2) among oxidized basalt scoria and the preserved landforms.

Range demonstrate that active magmatism has recently resumed in the region. Preliminary geochemical data from Jumbo Dome lavas suggest adakite-like characteristics (Cameron et al., 2015). Similarly, adakite-like geochemical signatures are common in Wrangell arc lavas of all ages and have been attributed to melting along the edge of the Yakutat slab (Brueseke et al., 2019). Considering the northeastern extent of subducted Yakutat slab from a recent geophysical compilation (Pavlis et al., 2019), it is clear that the Quaternary lava flows along the southern flank of the eastern Alaska Range are located above the edge of the slab (Fig. 1) and their petrogenesis is thus likely also influenced by the slab edge. Due to the observation that the as yet unsubducted portion of the Yakutat slab is thicker than the imaged subducted section (~30 km vs. ~17 km), Gulick et al. (2013) postulated that an enhanced stage of collision between the Yakutat microplate and southern Alaska began at ca. 1 Ma. We further hypothesize that the introduction of the thicker Yakutat crust led to an increase in end loading during the Quaternary, which may have facilitated tearing of the Yakutat slab (Fuis et al., 2008) or an increase in slab dip without tearing (Pavlis et al., 2019), a lull in Wrangell arc magmatism after 200,000 ka (Richter et al., 1990), and the revival of Alaska Range magmatism. Our preliminary, yet cursory, documentation of Quaternary lavas in the eastern Alaska Range provides a foundation for future detailed petrologic and geochemical studies to address their origin.

5.3. Upper plate response to oblique flat slab subduction of the Yakutat oceanic plateau in southern Alaska

The compiled regional thermochronology dataset from southern Alaska reflects widespread, yet spatially heterogeneous, ca. 30 Ma-to-present cooling, bedrock exhumation, and topographic growth

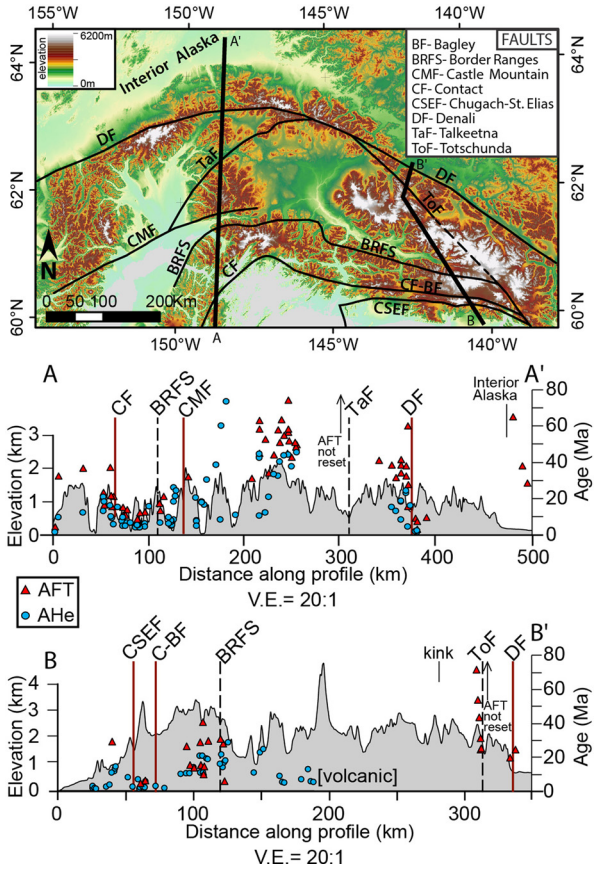

Fig. 5. Topographic-cooling age profiles showing that young bedrock apatite fission-track (AFT) and apatite (U-Th)/He (AHe) cooling ages are spatially associated with major Cenozoic strike-slip fault systems in southern Alaska. Profile A-A′ is modified from Terhune et al. (2019). Cooling age data are compiled from Terhune et al. (2019 and references therein), Arkle et al. (2013 and references therein), Berger et al. (2008), Enkelmann et al. (2015 and references therein), O'Sullivan and Currie (1996), Meigs et al. (2008), Spotila et al. (2004), Riccio et al. (2014), and Benowitz et al. (2014). "AFT not reset" refers to AFT ages that are older than 80 Ma. Red faults on the profiles have Neogene activity, whereas faults indicated by a broken line have no documented Neogene activity.

focused along preexisting active strike-slip fault systems (Fig. 6). In the proximal hanging wall of the flat slab collision zone, deep and rapid exhumation in the St. Elias Mountains is mainly focused in the syntaxis region (Fig. 1A). In the syntaxis, localized motion on the dextral transpressional Fairweather fault transitions to convergence across the thrust belt (Chapman et al., 2012). Residual relative plate motion is bifurcated northward to the Denali fault system (Fig. 1B) and westward to the Chugach-St. Elias fault and eastern end of the Contact fault, which was renamed as the Bagley fault (Bruhn et al., 2012; Enkelmann et al., 2015). The Fairweather, Chugach-St. Elias, and Bagley faults accommodated margin-parallel translation of the Yakutat terrane relative to North America throughout the Cenozoic (Bruhn et al., 2012; Lease et al., 2021) and were thus active throughout the onset of Yakutat flat slab subduction. To the north, rock uplift and exhumation in the Alaska Range has been focused along the dextral transpressional Denali fault system since ca. 30 Ma (Lease et al., 2016). Prior to ca. 30 Ma, the Denali fault accommodated mainly lateral motion of outboard terranes, which transitioned to transpression upon introduction of the Yakutat flat slab at ca. 30 Ma (e.g., Finzel et al., 2016; Waldien et al., 2021b). Near the apex of the Alaska orocline, localized recent exhumation in the high peak regions of the northern Chugach Mountains (Mt. Marcus Baker–MB on Fig. 1) and southern Talkeetna Mountains (east of Hatcher Pass–HP on Fig. 1) has been attributed to Oligocene-Neogene slip on the Castle Mountain fault, Contact fault, and subsidiary structures in the Matanuska Valley, which likely were active during initial subduction of the Yakutat oceanic plateau (Arkle et al., 2013 and references therein; Terhune et al., 2019).

One peculiar aspect of the upper plate structural configuration is that major inactive structures, despite their importance as significant geologic-geophysical boundaries, appear to have experienced limited reactivation upon the transition to the flat slab setting. For example, the Talkeetna and Border Ranges faults are the two most profound geophysical features in southern Alaska and likely penetrate the lithosphere (Miller et al., 2018), yet the only sections of these faults with demonstrable Neogene slip are the sections near the aforementioned active strike-slip fault systems (Waldien et al., 2021a). Cooling age profiles that span the inherited active and inactive structures clearly show that bedrock cooling ages increase with distance away from the currently active transpressional fault systems toward unreactivated inherited structures and sedimentary basins (Fig. 5).

Four long-lived and still active sedimentary basin systems (Copper River, Tanana, Susitna, Cook Inlet–Fig. 1A) were active prior to, and during, flat slab subduction of the Yakutat oceanic plateau (Trop and Ridgway, 2007). Flexural subsidence in response to tectonic drivers likely controls depocenter locations and stability (Ridgway et al., 2007). Additionally, the location of the Cook Inlet basin has been correlated with dynamic subsidence in relation to the geometry of the subducted slab (Haeussler and Saltus, 2011). Between the eastern Alaska Range and northern St. Elias Mountains, sparse geodetic data (Freymueller et al., 2008) suggest that a small amount of regional shortening may accompany flexural subsidence in the Copper River basin, where active shortening structures have not been identified. Whereas protracted subsidence has created accommodation space near the relatively stable basin axes since at least the Eocene (Trop and Ridgway, 2007), evidence for basin inversion is present along the boundaries of the active basins (e.g., Finzel et al., 2011a; Saltus et al., 2016) and has been linked to outward growth of topography in response to slip on range-front shortening structures splaying from the master Denali fault (e.g., Haeussler, 2008; Bemis et al., 2015; Haeussler et al., 2017; Waldien et al., 2018; Allen et al., 2021). Topographic growth associated with the shortening structures led to widespread drainage reorganization throughout southern Alaska (Finzel et al., 2016; Benowitz et al., 2019), which resulted in isolated active basins separated by high relief regions centered on the active transpression zones (Figs. 1A and 6).

Southern Alaska experienced a wholesale refocusing of arc magmatism after ca. 32 Ma, which we interpret as a result of the onset of flat slab subduction of the Yakutat oceanic plateau (Fig. 6). Regional pluton ages indicate that arc magmatism prior to ca. 32 Ma was focused along the Denali fault (Trop et al., 2019). After restoring ca. 30 Myr of slip on the Denali fault (Regan et al., 2021; Waldien et al., 2021b), magmatism along the Denali fault appears to record an arc-trench (trench inferred to be the Chugach-St. Elias fault–Fig. 1) gap of ~200-450 km. The potentially large arc-trench gap prior to ca. 32 Ma may imply a component of shallow subduction prior to the Yakutat flat slab and/or that the Denali fault served as a conduit for underplated mantle-derived melts. The observed decline in Alaska Range arc magmatism from ca. 30 to 25 Ma is contemporaneous with the birth of the Wrangell arc at ca. 30 Ma, and both are generally interpreted to record initial subduction of the Yakutat oceanic plateau (Brueseke et al., 2019; Trop et al., 2019; Jones et al., 2021). Throughout its ca. 30 Myr duration, the Wrangell arc has been focused within a region of precursor upper plate strike-slip faulting (the Totschunda fault) above the northeastern edge of the Yakutat slab (Trop et al., 2021). The newly recognized Quaternary volcanic field in the eastern Alaska Range (Figs. 1A and 4) also coincides with the imaged northeastern edge

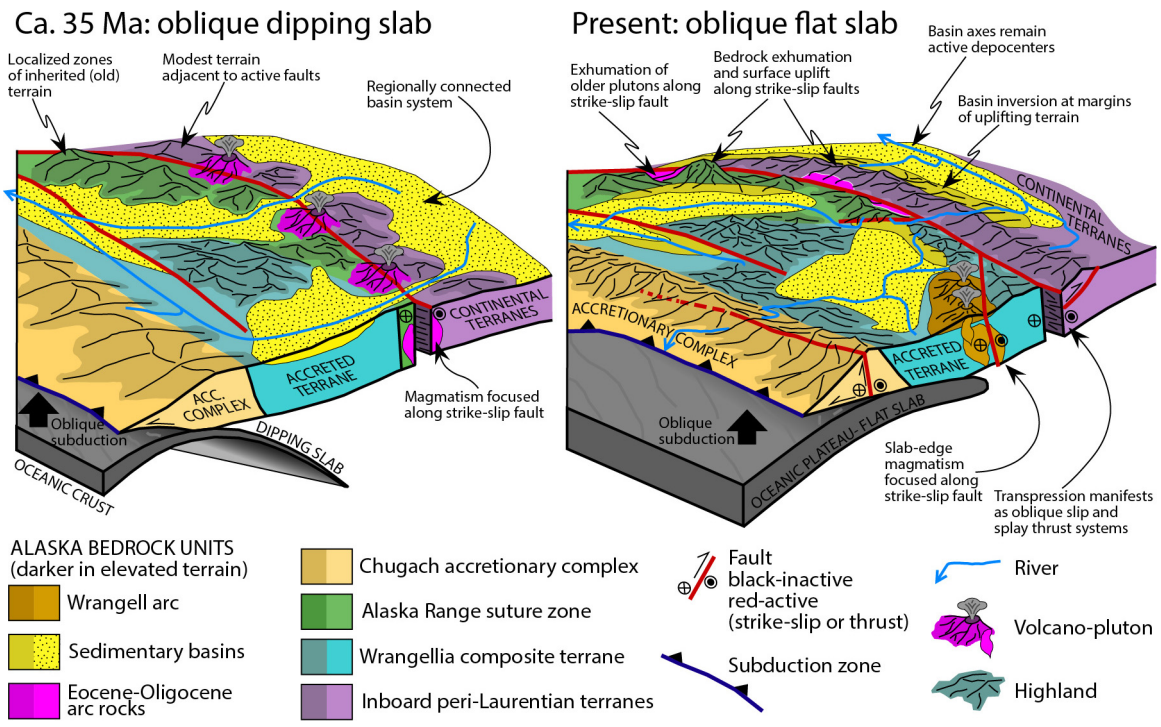

Fig. 6. Schematic diagrams showing the ca. 32-0 Ma southern Alaska tectonic evolution as it displays salient features of "normal" (left) and flat slab (right) subduction in obliquely convergent environments. Key features of the tectonic evolution upon the onset of oblique flat slab subduction include (1) active strike-slip fault systems transition into transpressional deformation zones with bedrock cooling/exhumation/surface uplift focused along the fault systems; (2) topographic growth associated with transpression zones causes drainage reorganization and inversion along the edges of basins; and (3) magmatism is focused above the slab edge and active strike-slip fault systems play a role in facilitating magma ascent. Paleo-drainage directions are inferred from Finzel et al. (2016) and Trop and Ridgway (2007).

of the subducted Yakutat slab (Pavlis et al., 2019) and magma ascent may have been facilitated by deep-seated structures associated with the Denali fault system. These observations together suggest that the northeastern margin geometry of the Yakutat slab has remained relatively stable with respect to the upper plate south of the Denali fault from ca. 30-1 Ma.

The sum of the compiled data and associated interpretations leads to a set of salient features describing the upper plate geologic evolution in response to oblique subduction of the Yakutat oceanic plateau beneath southern Alaska. These features are portrayed in Fig. 6 and include (1) bedrock exhumation and topographic development are focused along strike-slip fault systems that were active at the time of slab flattening; (2) foreland basin inversion is restricted to the periphery of regions of growing topographic relief; and (3) arc magmatism refocuses into the region above the slab edge, and the loci of volcanism are spatially associated with active strike-slip fault systems.

5.4. The role of preexisting upper plate strike-slip faults in the tectono-magmatic response to oblique subduction of oceanic plateaus

The geophysical and geological datasets summarized herein show that the post-30 Ma patterns of bedrock exhumation, magmatism, and sedimentation in southern Alaska provide an archive of oblique subduction of an oceanic plateau. Our analysis suggests that obliquely convergent margins with preexisting upper plate strike-slip structures experiencing oblique flat slab subduction will undergo focused bedrock exhumation and associated topographic growth along major strike-slip structures that were active prior to, and during, the slab flattening process. Increased upper plate convergence appears to have the effect of transitioning the active fault systems from transcurrent to transpressional kinematics rather than wholesale reactivation of inactive structures. Magmatism during the oblique flat slab regime will not necessarily migrate inboard as has been documented along other flat slab convergent margins (e.g., central Chile-Argentina–Capaldi et al., 2020), but instead melting may be focused along the lateral edge of the slab, and magma ascent through the upper plate may be facilitated by active lithospheric-scale strike-slip fault systems. A key outcome from our analysis is that upper plate strike-slip faults systems are loci of bedrock cooling, magmatism, and topographic growth, all of which favor block-style deformation models wherein the size of the blocks is controlled by the spacing of the inherited strike-slip fault systems.

Modern and ancient examples of oblique subduction of oceanic plateaus share similarities with our documentation of the Oligocene-to-present evolution of southern Alaska. Active oblique subduction of the Samoan and Louisville Ridges into the Tonga Trench has led to loci of upper plate convergence, strike-slip faulting, and focusing of magmatism into upper plate structures, which sets these sections of the margin apart from the otherwise extensional upper plate (Pelletier et al., 1998). In the northern Andes of Ecuador and Colombia, protracted slip histories alternating between transpressional and transtensional deformation within upper plate strike-slip fault systems appear to record changes in the obliquity, thickness, and dip (inferred from upper plate convergence) of subducting slabs throughout the Cenozoic (e.g., Mora et al., 2017 and references therein). Here, multiple angular unconformities associated with changes in sediment provenance recorded in basin strata adjacent to the strike-slip fault systems suggest that basin inversion and magmatism were focused along preexisting lithospheric-scale structures that were active during changes in the upper plate deformation regime (Mora et al., 2017 and references therein). Lastly, the Late Cretaceous upper plate tectonic setting of western North America at the latitude of the contiguous United States involved a regional intra-arc strike-slip fault system that accommodated oblique convergence and aided in magma ascent (e.g., Tikoff and de Saint Blanquat, 1997, among several oth-

ers). The kinematics of the intra-arc shear system evolved with changes in the convergence angle and rate (Nadin et al., 2016) until inferred slab flattening related to oblique subduction of a hypothesized oceanic plateau exhumed the batholith as deformation and magmatism migrated inboard (e.g., Saleeby, 2003). Shortening and focused cooling of the upper plate took place along preexisting structures, some of which were strike-slip faults that were active at the onset of plateau oblique subduction (e.g., Nadin et al., 2016).

Given the abundance of oceanic plateaus on the modern seafloor (e.g., Mann and Taira, 2004), the correlation between oceanic plateau subduction and shallow slab dip (e.g., Gutscher et al., 2000), and the observation that nearly all plate boundaries have some amount of obliquity (e.g., Philippon and Corti, 2016), it follows that oblique flat slab subduction of oceanic plateaus is a fundamental, yet often overlooked, geologic process. Moreover, the upper plate geologic evolution resulting from slab flattening in a partitioned oblique subduction setting shows a noteworthy departure from the upper plate evolution in orthogonal flat slab regions (e.g., Mexico–Arce et al., 2020; Costa Rica–Gardner et al., 2013; Peru–Bishop et al., 2017) and in oblique flat slab environments without active preexisting continental scale strike-slip faults (e.g., Ontong Java–Mann and Taira, 2004, central Argentina–Siame et al., 2005). Variability in the tectonic behavior among the examples discussed herein suggests that the precursor upper plate geologic history in each region partly controls the resulting geologic evolution in response to oblique flat slab subduction.

6. Conclusion

We have shown herein that the post-30 Ma tectono-magmatic evolution of southern Alaska can be linked to oblique flat slab subduction of an oceanic plateau and propose that southern Alaska is an archetypical example of such a process. Key outcomes from our study include the following:

1) Post-30 Ma bedrock cooling and exhumation are widespread in the eastern Alaska Range. Most of the post-30 Ma bedrock cooling and interpreted topographic growth are associated with transpression in the Denali fault system. Quaternary cooling in the eastern Alaska Range is best explained by thermal effects related to ca. 1 Ma volcanism.
2) The youngest cooling ages across southern Alaska are spatially associated with regions of high topographic relief adjacent to major strike-slip fault systems. Increased upper plate convergence related to subduction of the Yakutat oceanic plateau is focused on the preexisting strike-slip fault systems that were active at the time of slab flattening. The shift to oblique flat slab subduction had the effect of changing the bulk deformation regime within the strike-slip fault systems from transcurrent to transpressional. Inherited structures that were inactive at the time of slab flattening appear to have been reactivated only near the active lithospheric scale transpressional fault systems.
3) Regional drainage networks were reorganized during subduction of the Yakutat flat slab. Basins were isolated by inversion along their margins where topography developed in response to transpressional deformation, but the basin axes remain active depocenters.
4) Subduction of the Yakutat oceanic plateau is associated with the demise of subduction-related magmatism along the Denali fault at ca. 32-25 Ma and the refocusing of arc magmatism above the northeastern edge of the slab after ca. 30 Ma. Arc magmatism was spatially associated with active strike-slip fault systems during both time intervals.
5) Quaternary volcanism in the eastern Alaska Range records the resumption of magmatism in central Alaska after a ca. 24 Myr hiatus and is focused above the Yakutat slab edge. We interpret that the revival of Alaska Range magmatism is related to a recent (ca. 1 Ma) change in Yakutat slab geometry or a slab tear, possibly in response to the introduction of a thicker portion of the plateau to the southern Alaska margin.
6) The precursor geologic history of the upper plate plays an important role in the way that upper plate deformation is manifested, and magmatism is focused during changes to margin obliquity and dip of the subducting slab.

CRediT authorship contribution statement

T.S. Waldien: Conceptualization, Formal analysis, Writing – original draft. **R.O. Lease:** Supervision, Writing – review & editing. **S.M. Roeske:** Funding acquisition, Supervision, Writing – review & editing. **J.A. Benowitz:** Investigation, Writing – review & editing. **P.B. O'Sullivan:** Investigation.

Declaration of competing interest

The authors declare that they have no known competing financial interests or personal relationships that could have appeared to influence the work reported in this paper.

Acknowledgements

This work was funded by an INTERN supplement to an NSF Tectonics award #EAR-1828737 (Roeske), #EAR-1828023 (Benowitz), and the U.S. Geological Survey Mineral Resources Program (Lease). We are grateful to 40 Mile Air for transportation during sample collection. The manuscript benefited from constructive comments by Peter Haeussler, Marti Miller, Eric Cowgill, and two anonymous reviewers. Any use of trade, firm, or product names is for descriptive purposes only and does not imply endorsement by the U.S. Government.

Appendix. Supplementary material

Supplementary material related to this article can be found online at https://doi.org/10.1016/j.epsl.2021.117242.

References

Allam, A.A., Schulte-Pelkum, V., Ben-Zion, Y., Tape, C., Ruppert, N., Ross, Z.E., 2017. Ten kilometer vertical Moho offset and shallow velocity contrast along the Denali fault zone from double-difference tomography, receiver functions, and fault zone head waves. Tectonophysics 721, 56–69.

Allen, W.K., Ridgway, K.D., Benowitz, J.A., Waldien, T.S., Roeske, S.M., Fitzgerald, P.G., Gillis, R.J., 2021. Neogene sedimentary record of the evolution of a translated strike-slip basin along the Denali fault system: implications for timing of displacement, composite basin development, and regional tectonics of southern Alaska. Geosphere. https://doi.org/10.1130/GES02435.1, in press.

Andronikov, A.V., Mukasa, S.B., 2010. $^{40}Ar/^{39}Ar$ eruption ages and geochemical characteristics of late Tertiary to Quaternary intraplate and arc-related lavas in interior Alaska. Lithos 115 (1–4), 1–14.

Arce, J.L., Ferrari, L., Morales-Casique, E., Vasquez-Serrano, A., Arroyo, S.M., Layer, P.W., Benowitz, J., López-Martínez, M., 2020. Early Miocene arc volcanism in the Mexico City Basin: inception of the Trans-Mexican volcanic belt. J. Volcanol. Geotherm. Res. 408, 107104.

Arkle, J.C., Armstrong, P.A., Haeussler, P.J., Prior, M.G., Hartman, S., Sendziak, K.L., Brush, J.A., 2013. Focused exhumation in the syntaxis of the western Chugach Mountains and Prince William Sound, Alaska. Geol. Soc. Am. Bull. 125 (5–6), 776–793.

Axen, G.J., van Wijk, J.W., Currie, C.A., 2018. Basal continental mantle lithosphere displaced by flat-slab subduction. Nat. Geosci. 11 (12), 961–964.

Bemis, S.P., Weldon, R.J., Carver, G.A., 2015. Slip partitioning along a continuously curved fault: quaternary geologic controls on Denali fault system slip partitioning, growth of the Alaska Range, and the tectonics of south-central Alaska. Lithosphere 7 (3), 235–246.

Benowitz, J.A., Davis, K., Roeske, S., 2019. A river runs through it both ways across time: $^{40}Ar/^{39}Ar$ detrital and bedrock muscovite geochronology constraints on the Neogene paleodrainage history of the Nenana River system, Alaska Range. Geosphere 15 (3), 682–701.

Benowitz, J.A., Haeussler, P.J., Layer, P.W., O'Sullivan, P.B., Wallace, W.K., Gillis, R.J., 2012. Cenozoic tectono-thermal history of the Tordrillo Mountains, Alaska: Paleocene-Eocene ridge subduction, decreasing relief, and late Neogene faulting. Geochem. Geophys. Geosyst. 13 (4).

Benowitz, J.A., Layer, P.W., Vanlaningham, S., 2014. Persistent long-term (c. 24 Ma) exhumation in the eastern Alaska Range constrained by stacked thermochronology. Geol. Soc. (Lond.) Spec. Publ. 378 (1), 225–243.

Berger, A.L., Spotila, J.A., Chapman, J.B., Pavlis, T.L., Enkelmann, E., Ruppert, N.A., Buscher, J.T., 2008. Architecture, kinematics, and exhumation of a convergent orogenic wedge: a thermochronological investigation of tectonic–climatic interactions within the central St. Elias orogen, Alaska. Earth Planet. Sci. Lett. 270 (1–2), 13–24.

Bill, N.S., Mix, H.T., Clark, P.U., Reilly, S.P., Jensen, B.J., Benowitz, J.A., 2018. A stable isotope record of late Cenozoic surface uplift of southern Alaska. Earth Planet. Sci. Lett. 482, 300–311.

Bishop, B.T., Beck, S.L., Zandt, G., Wagner, L., Long, M., Antonijevic, S.K., Kumar, A., Tavera, H., 2017. Causes and consequences of flat-slab subduction in southern Peru. Geosphere 13 (5), 1392–1407.

Brueseke, M.E., Benowitz, J.A., Trop, J.M., Davis, K.N., Berkelhammer, S.E., Layer, P.W., Morter, B.K., 2019. The Alaska Wrangell Arc: ∼30 Ma of subduction-related magmatism along a still active arc-transform junction. Terra Nova 31 (1), 59–66.

Bruhn, R.L., Sauber, J., Cotton, M.M., Pavlis, T.L., Burgess, E., Ruppert, N., Forster, R.R., 2012. Plate margin deformation and active tectonics along the northern edge of the Yakutat Terrane in the Saint Elias orogen, Alaska, and Yukon, Canada. Geosphere 8 (6), 1384–1407.

Cameron, C.E., Nye, C.J., Bull, K.F., Woods, Rebecca-Ellen, 2015. Jumbo Dome, interior Alaska: whole-rock, major- and trace-element analyses. Alaska Division of Geological & Geophysical Surveys Raw Data File 2015-14, p. 3.

Capaldi, T.N., Horton, B.K., McKenzie, N.R., Mackaman-Lofland, C., Stockli, D.F., Ortiz, G., Alvarado, P., 2020. Neogene retroarc foreland basin evolution, sediment provenance, and magmatism in response to flat slab subduction, western Argentina. Tectonics 39 (7), e2019TC005958.

Chapman, J.B., Pavlis, T.L., Bruhn, R.L., Worthington, L.L., Gulick, S.P., Berger, A.L., 2012. Structural relationships in the eastern syntaxis of the St. Elias orogen, Alaska. Geosphere 8 (1), 105–126.

Christeson, G.L., Gulick, S.P., van Avendonk, H.J., Worthington, L.L., Reece, R.S., Pavlis, T.L., 2010. The Yakutat terrane: dramatic change in crustal thickness across the Transition fault, Alaska. Geology 38 (10), 895–898.

Donelick, R.A., O'Sullivan, P.B., Ketcham, R.A., 2005. Apatite fission-track analysis. Rev. Mineral. Geochem. 58 (1), 49–94.

Elliott, J., Freymueller, J.T., 2020. A block model of present-day kinematics of Alaska and western Canada. J. Geophys. Res., Solid Earth 125 (7), e2019JB018378.

Enkelmann, E., Koons, P.O., Pavlis, T.L., Hallet, B., Barker, A., Elliott, J., Garver, J.I., Gulick, S.P., Headley, R.M., Pavlis, G.L., Ridgway, K.D., Ruppert, N., Har, J.A., Van Avendonk, H.J., 2015. Cooperation among tectonic and surface processes in the St. Elias Range, Earth's highest coastal mountains. Geophys. Res. Lett. 42 (14), 5838–5846.

Enkelmann, E., Sanchez Lohff, S.K., Finzel, E.S., 2019. Detrital zircon double-dating of forearc basin strata reveals magmatic, exhumational, and thermal history of sediment source areas. Geol. Soc. Am. Bull. 131 (7–8), 1364–1384. https://doi.org/10.1130/B35043.1.

Espurt, N., Funiciello, F., Martinod, J., Guillaume, B., Regard, V., Faccenna, C., Brusset, S., 2008. Flat subduction dynamics and deformation of the South American plate: insights from analog modeling. Tectonics 27 (3).

Estéve, C., Audet, P., Schaeffer, A.J., Schutt, D., Aster, R.C., Cubley, J., 2020. The upper mantle structure of northwestern Canada from teleseismic body wave tomography. J. Geophys. Res., Solid Earth 125 (2), e2019JB018837.

Falkowski, S., Enkelmann, E., 2016. Upper-crustal cooling of the Wrangellia composite terrane in the northern St. Elias Mountains, western Canada. Lithosphere 8 (4), 359–378.

Falkowski, S., Enkelmann, E., Ehlers, T.A., 2014. Constraining the area of rapid and deep-seated exhumation at the St. Elias syntaxis, Southeast Alaska, with detrital zircon fission-track analysis. Tectonics 33 (5), 597–616.

Finzel, E.S., Enkelmann, E., Falkowski, S., Hedeen, T., 2016. Long-term fore-arc basin evolution in response to changing subduction styles in southern Alaska. Tectonics 35 (7), 1735–1759.

Finzel, E.S., Flesch, L.M., Ridgway, K.D., 2011b. Kinematics of a diffuse North America–Pacific–Bering plate boundary in Alaska and western Canada. Geology 39 (9), 835–838.

Finzel, E.S., Trop, J.M., Ridgway, K.D., Enkelmann, E., 2011a. Upper plate proxies for flat-slab subduction processes in southern Alaska. Earth Planet. Sci. Lett. 303 (3–4), 348–360.

Fitzgerald, P.G., Roeske, S.M., Benowitz, J.A., Riccio, S.J., Perry, S.E., Armstrong, P.A., 2014. Alternating asymmetric topography of the Alaska range along the strike-slip Denali fault: strain partitioning and lithospheric control across a terrane suture zone. Tectonics 33 (8), 1519–1533.

Fitzgerald, P.G., Sorkhabi, R.B., Redfield, T.F., Stump, E., 1995. Uplift and denudation of the central Alaska Range: a case study in the use of apatite fission track thermochronology to determine absolute uplift parameters. J. Geophys. Res., Solid Earth 100 (B10), 20175–20191.

Freymueller, J.T., 2010. Active tectonics of plate boundary zones and the continuity of plate boundary deformation from Asia to North America. Curr. Sci., 1719–1732.

Freymueller, J.T., Woodard, H., Cohen, S.C., Cross, R., Elliott, J., Larsen, C.F., Hreinsdóttir, S., Zweck, C., 2008. Active deformation processes in Alaska, based on 15 years of GPS measurements. In: Active Tectonics and Seismic Potential of Alaska. In: AGU Monograph Series, vol. 179, pp. 1–42.

Fuis, G.S., Moore, T.E., Plafker, G., Brocher, T.M., Fisher, M.A., Mooney, W.D., Ruppert, N.A., 2008. Trans-Alaska Crustal Transect and continental evolution involving subduction underplating and synchronous foreland thrusting. Geology 36 (3), 267–270.

Galbraith, R., 2005. Statistics for Fission Track Analysis. Chapman & Hall / CRC, Boca Raton, FLA.

Gardner, T.W., Fisher, D.M., Morell, K.D., Cupper, M.L., 2013. Upper-plate deformation in response to flat slab subduction inboard of the aseismic Cocos Ridge, Osa Peninsula, Costa Rica. Lithosphere 5 (3), 247–264.

Gulick, S.P.S., Reece, R.S., Christeson, G.L., Van Avendonk, H., Worthington, L.L., Pavlis, T.L., 2013. Seismic images of the Transition fault and the unstable Yakutat–Pacific–North American triple junction. Geology 41 (5), 571–574.

Gulick, S.P., Jaeger, J.M., Mix, A.C., Asahi, H., Bahlburg, H., Belanger, C.L., Berbel, G.B., Childress, L., Cowan, E., Drab, L., Forwick, M., 2015. Mid-Pleistocene climate transition drives net mass loss from rapidly uplifting St. Elias Mountains, Alaska. Proc. Natl. Acad. Sci. 112 (49), 15042–15047.

Gutscher, M.A., Spakman, W., Bijwaard, H., Engdahl, E.R., 2000. Geodynamics of flat subduction: seismicity and tomographic constraints from the Andean margin. Tectonics 19 (5), 814–833.

Haeussler, P.J., 2008. An overview of the neotectonics of interior Alaska: far-field deformation from the Yakutat microplate collision. In: Freymueller, J.T., et al. (Eds.), Active Tectonics and Seismic Potential of Alaska, vol. 179. AGU, Washington, D.C., pp. 83–108.

Haeussler, P.J., Saltus, R.W., 2011. Location and extent of Tertiary structures in Cook Inlet basin, Alaska, and mantle dynamics that focus deformation and subsidence. U.S. Geological Survey Professional Paper 1776-D, 26 p.

Haeussler, P.J., O'sullivan, P., Berger, A.L., Spotila, J.A., 2008. Neogene exhumation of the Tordrillo Mountains, Alaska, and correlations with Denali (Mount McKinley). In: American Geophysical Union Geophysical Monograph Series, vol. 179, pp. 269–285.

Haeussler, P.J., Saltus, R.W., Stanley, R.G., Ruppert, N., Lewis, K., Karl, S.M., Bender, A., 2017. The Peters Hills basin, a Neogene wedge-top basin on the Broad Pass thrust fault, south-central Alaska. Geosphere 13 (5), 1464–1488.

Horikawa, K., Martin, E.E., Basak, C., Onodera, J., Seki, O., Sakamoto, T., Ikehara, M., Sakai, S., Kawamura, K., 2015. Pliocene cooling enhanced by flow of low-salinity Bering Sea water to the Arctic Ocean. Nat. Commun. 6 (7587), 1–9. https://doi.org/10.1038/ncomms8587.

Jadamec, M.A., Billen, M.I., Roeske, S.M., 2013. Three-dimensional numerical models of flat slab subduction and the Denali fault driving deformation in south-central Alaska. Earth Planet. Sci. Lett. 376, 29–42.

Jones III, J.V., Todd, E., Box, S.E., Haeussler, P.J., Holm-Denoma, C.S., Karl, S.M., Graham, G.E., Bradley, D.C., Kylander-Clark, A.R.C., Friedman, R.M., Layer, P.W., 2021. Cretaceous to Oligocene magmatic and tectonic evolution of the western Alaska Range: insights from U-Pb and $^{40}Ar/^{39}Ar$ geochronology. Geosphere 17 (1), 118–153.

Koons, P.O., Hooks, B.P., Pavlis, T., Upton, P., Barker, A.D., 2010. Three-dimensional mechanics of Yakutat convergence in the southern Alaskan plate corner. Tectonics 29. https://doi.org/10.1029/2009TC002463.

Lease, R.O., 2018. Pliocene erosional pulse and glacier-landscape feedbacks in the western Alaska Range. Earth Planet. Sci. Lett. 497, 62–68. https://doi.org/10.1016/j.epsl.2018.06.009.

Lease, R.O., Haeussler, P.J., O'Sullivan, P., 2016. Changing exhumation patterns during Cenozoic growth and glaciation of the Alaska Range: insights from detrital thermochronology and geochronology. Tectonics 35 (4), 934–955.

Lease, R.O., Haeussler, P.J., Witter, R.C., Stockli, D.F., Bender, A.M., Kelsey, H.M., O'Sullivan, P.B., 2021. Extreme Quaternary plate boundary exhumation and strike slip localized along the southern Fairweather fault, Alaska, USA. Geology 49 (5), 602–606.

Little, T.A., Naeser, C.W., 1989. Tertiary tectonics of the Border Ranges fault system, Chugach Mountains, Alaska: deformation and uplift in a forearc setting. J. Geophys. Res., Solid Earth 94 (B4), 4333–4359.

Mann, P., Taira, A., 2004. Global tectonic significance of the Solomon Islands and Ontong Java Plateau convergent zone. Tectonophysics 389 (3–4), 137–190.

Marshak, S., Karlstrom, K., Timmons, J.M., 2000. Inversion of Proterozoic extensional faults: an explanation for the pattern of Laramide and Ancestral Rockies intracratonic deformation, United States. Geology 28 (8), 735–738.

McDermott, R.G., Ault, A.K., Caine, J.S., Thomson, S.N., 2019. Thermotectonic history of the Kluane Ranges and evolution of the eastern Denali fault zone in southwestern Yukon, Canada. Tectonics 38 (8), 2983–3010.

Meigs, A., Johnston, S., Garver, J., Spotila, J., 2008. Crustal-scale structural architecture, shortening, and exhumation of an active, eroding orogenic wedge (Chugach/St Elias Range, southern Alaska). Tectonics 27 (4).

Miller, M.S., O'Driscoll, L.J., Porritt, R.W., Roeske, S.M., 2018. Multiscale crustal architecture of Alaska inferred from P receiver functions. Lithosphere 10 (2), 267–278.

Mora, J.A., Oncken, O., Le Breton, E., Ibánez-Mejia, M., Faccenna, C., Veloza, G., Veléz, V., de Freitas, M., Mesa, A., 2017. Linking Late Cretaceous to Eocene tectonostratigraphy of the San Jacinto fold belt of NW Colombia with Caribbean Plateau collision and flat subduction. Tectonics 36 (11), 2599–2629.

Nadin, E.S., Saleeby, J., Wong, M., 2016. Thermal evolution of the Sierra Nevada batholith, California, and implications for strain localization. Geosphere 12 (2), 377–399.

O'Sullivan, P.B., Currie, L.D., 1996. Thermotectonic history of Mt Logan, Yukon Territory, Canada: implications of multiple episodes of middle to late Cenozoic denudation. Earth Planet. Sci. Lett. 144 (1–2), 251–261.

Pavlis, G.L., Bauer, M.A., Elliott, J.L., Koons, P., Pavlis, T.L., Ruppert, N., Worthington, L.L., 2019. A unified three-dimensional model of the lithospheric structure at the subduction corner in southeast Alaska: summary results from STEEP. Geosphere 15 (2), 382–406.

Pelletier, B., Calmant, S., Pillet, R., 1998. Current tectonics of the Tonga–New Hebrides region. Earth Planet. Sci. Lett. 164 (1–2), 263–276.

Philippon, M., Corti, G., 2016. Obliquity along plate boundaries. Tectonophysics 693, 171–182.

Ramos, V.A., Cristallini, E.O., Pérez, D.J., 2002. The Pampean flat-slab of the Central Andes. J. South Am. Earth Sci. 15 (1), 59–78.

Regan, S.P., Benowitz, J.A., Holland, M.E., 2020. A plutonic brother from another magma mother: disproving the Eocene Foraker-McGonagall pluton piercing point and implications for long-term slip on the Denali Fault. Terra Nova 32 (1), 66–74.

Regan, S., Benowitz, J.B., Waldien, T.S., Holland, M., Roeske, S.M., O'Sullivan, P.B., Layer, P., 2021. Long distance plutonic relationships demonstrate 33 million years of strain partitioning along the Denali fault. Terra Nova. https://doi.org/10.1111/ter.12555, in press.

Renne, P.R., Mundil, R., Balco, G., Min, K., Ludwig, K.R., 2010. Joint determination of ^{40}K decay constants and ^{40}Ar*/^{40}K for the Fish Canyon sanidine standard, and improved accuracy for ^{40}Ar/^{39}Ar geochronology. Geochim. Cosmochim. Acta 74 (18), 5349–5367.

Riccio, S.J., Fitzgerald, P.G., Benowitz, J.A., Roeske, S.M., 2014. The role of thrust faulting in the formation of the eastern Alaska Range: thermochronological constraints from the Susitna Glacier thrust fault region of the intracontinental strike-slip Denali fault system. Tectonics 33 (11), 2195–2217.

Richter, D.H., Smith, J.G., Lanphere, M.A., Dalrymple, G.B., Reed, B.L., Shew, N., 1990. Age and progression of volcanism, Wrangell volcanic field, Alaska. Bull. Volcanol. 53 (1), 29–44.

Ridgway, K.D., Thoms, E.E., Layer, P.W., Lesh, M.E., White, J.M., Smith, S.V., 2007. Neogene transpressional foreland basin development on the north side of the central Alaska Range, Usibelli Group and Nenana Gravel, Tanana basin. In: Ridgway, K.D., Trop, J.M., Glen, J.M.G., O'Neill, J.M. (Eds.), Tectonic Growth of a Collisional Continental Margin: Crustal Evolution of Southern Alaska, vol. 431. Geological Society of America, Boulder, Colorado, pp. 507–548.

Roeske, S.M., Snee, L.W., Pavlis, T.L., Sisson, V.B., 2003. Dextral-slip reactivation of an arc-forearc boundary during Late Cretaceous-early Eocene oblique convergence in the northern Cordillera. In: Sisson, V.B., Roeske, S.M., Pavlis, T.L. (Eds.), Geology of a Transpressional Orogen Developed During Ridge-Trench Interaction Along the North Pacific Margin, vol. 371. Geological Society of America, Boulder, Colorado, pp. 141–170.

Ruppert, N.A., Ridgway, K.D., Freymueller, J.T., Cross, R.S., Hansen, R.A., 2008. Active tectonics of interior Alaska: seismicity, GPS geodesy, and local geomorphology. In: American Geophysical Union Geophysical Monograph Series, vol. 179, pp. 109–133.

Saleeby, J., 2003. Segmentation of the Laramide slab—evidence from the southern Sierra Nevada region. Geol. Soc. Am. Bull. 115 (6), 655–668.

Saltus, R.W., Stanley, R.G., Haeussler, P.J., Jones III, J.V., Potter, C.J., Lewis, K.A., 2016. Late Oligocene to present contractional structure in and around the Susitna basin, Alaska—geophysical evidence and geological implications. Geosphere 12 (5), 1378–1390.

Siame, L.L., Bellier, O., Sébrier, M., Araujo, M., 2005. Deformation partitioning in flat subduction setting: case of the Andean foreland of western Argentina (28 S–33 S). Tectonics 24 (5).

Spotila, J.A., Buscher, J.T., Meigs, A.J., Reiners, P.W., 2004. Long-term glacial erosion of active mountain belts: example of the Chugach–St. Elias Range, Alaska. Geology 32 (6), 501–504.

Stout, J.H., 1976. Geology of the Eureka Creek area, east-central Alaska Range. State of Alaska, Department of Natural Resources, Division of Geological & Geophysical Surveys Geologic Report 46. 32 pp., 1 sheet, scale 1:63,360.

Terhune, P.J., Benowitz, J.A., Trop, J.M., O'Sullivan, P.B., Gillis, R.J., Freymueller, J.T., 2019. Cenozoic tectono-thermal history of the southern Talkeetna Mountains, Alaska: insights into a potentially alternating convergent and transform plate margin. Geosphere 15 (5), 1539–1576.

Tikoff, B., de Saint Blanquat, M., 1997. Transpressional shearing and strike-slip partitioning in the Late Cretaceous Sierra Nevada magmatic arc, California. Tectonics 16 (3), 442–459.

Trop, J.M., Ridgway, K.D., 2007. Mesozoic and Cenozoic tectonic growth of southern Alaska: a sedimentary basin perspective. In: Ridgway, K.D., Trop, J.M., Glen, J.M.G., O'Neill, J.M. (Eds.), Tectonic Growth of a Collisional Continental Margin: Crustal Evolution of Southern Alaska, vol. 431. Geological Society of America, Boulder, Colorado, pp. 55–94.

Trop, J.M., Benowitz, J., Cole, R.B., O'Sullivan, P., 2019. Cretaceous to Miocene magmatism, sedimentation, and exhumation within the Alaska Range suture zone: a polyphase reactivated terrane boundary. Geosphere 15 (4), 1066–1101.

Trop, J.M., Benowitz, J.A., Kirby, C.S., Brueseke, M.E., 2021. Geochronology of the Wrangell Arc: spatial-temporal evolution of slab edge magmatism along a flat slab subduction-transform transition, Alaska-Yukon. Geosphere. https://doi.org/10.1130/GES02417.1, in press.

Twelker, E., Waldien, T.S., Newberry, R.J., Freeman, L.K., Sicard, K.R., Lande, L.L., Wypych, A., Reioux, D.A., Bachmann, E.N., 2020. Bedrock geologic map of the eastern Denali Highway area, Mount Hayes, Healy, and Talkeetna Mountains quadrangles, Alaska. Alaska Division of Geological & Geophysical Surveys Report of Investigation 2020-7: 1 sheet, 1:100,000 scale.

Vermeesch, P., 2012. On the visualisation of detrital age distributions. Chem. Geol. 312, 190–194.

Waldien, T.S., Roeske, S.M., Benowitz, J.A., Twelker, E., Miller, M.S., 2021a. Oligocene-Neogene lithospheric-scale reactivation of Mesozoic terrane accretionary structures in the Alaska Range suture zone, southern Alaska, USA. Geol. Soc. Am. Bull. 133 (3–4), 691–716.

Waldien, T.S., Roeske, S.M., Benowitz, J.A., 2021b. Tectonic underplating and dismemberment of the Maclaren-Kluane schist records Late Cretaceous terrane accretion polarity and ∼480 km of post-52 Ma dextral displacement on the Denali fault. Tectonics 40, e2020TC006677. https://doi.org/10.1029/2020TC006677.

Waldien, T.S., Roeske, S.M., Benowitz, J.A., Allen, W.K., Ridgway, K.D., O'Sullivan, P.B., 2018. Late Miocene to Quaternary evolution of the McCallum Creek thrust system, Alaska: insights for range-boundary thrusts in transpressional orogens. Geosphere 14 (6), 2379–2406.